Numerical Simulation of Bi-Materials Laser Densification

K. Dai[1], P. Klemens[2], and L. Shaw[1]

[1] Department of Metallurgy and Materials Engineering
[2] Department of Physics
Institute of Materials Science
University of Connecticut, Storrs, CT 06269

Abstract

The dominant procedure currently used for permanent fixed prosthodontics is porcelain-fused-to-metal (PFM) restoration that is a time consuming and labor intensive process. To address these shortcomings, this project will develop a solid freeform fabrication (SFF) technique for dental restoration. Thus, a dental restoration can be built from a computer model without part-specific tooling and human intervention. The SFF technique to be developed is called multi-materials laser densification (MMLD) and capable of dealing with multiple dental materials such as dental alloys and porcelains. In order to provide guidelines for laser densification of multiple materials, numerical simulation has been carried out using the ANSYS code with 3-dimensional elements to model the temperature and stress fields during the MMLD process. Effects of laser scanning patterns and scanning rates have been investigated. Implications of these results on laser densification of multiple materials are discussed.

Keywords: Solid freeform fabrication, Dental restoration, Laser densification, Finite element modeling, Thermal and stress analyses.

Introduction

The dominant procedure currently used for permanent fixed prosthodontics is porcelain-fused-to-metal (PFM) restoration. In this procedure multiple materials and multiple processing steps are needed. As such, it is a time consuming and labor intensive process. However, the recent advancement in solid freeform fabrication (SFF) provides opportunities to carry out dental restorations from a computer model without part-specific tooling and human intervention, thereby reducing the labor cost and increasing the restoration rate. One of the potential approaches using SFF for dental restoration will be laser-assisted densification of multiple dental materials, or in short, multi-materials laser densification (MMLD). Obviously, there are many factors in MMLD that can affect the final quality of the restoration. These factors include material and processing issues such as types of materials used, the shape of the dental restoration, laser scanning pattern, scanning rate, and scanning spacing. For a specific restoration, many experiments are needed to optimize the fabrication process so that the maximum strength, minimum residual stress and distortion can be achieved. Such an experimental trial-and-error approach will inevitably lead to a high cost of the dental restoration through the MMLD process.

Recently, finite element method (FEM) has been increasingly used in many fields of fabrication to simulate and analyze the fabrication process. The reliability and efficiency of FEM have been well established. In this study we have utilized FEM to develop fundamental

understanding of temperature distribution, development of thermal transient and residual stresses, and distortion of the dental restoration during the MMLD process. Because of the involvement of multiple materials, the MMLD process is expected to be a very complicated process, especially when residual stresses and distortion are to be minimized. Thus, as the first step towards modeling complex-shaped multi-materials laser densification, simplified bi-materials laser densification has been investigated in this study. The numerical simulation was carried out using the ANSYS code and four different conditions of bi-materials laser densification were investigated.

Verification of 3D Model

To check the correctness of the 3D finite element models built in this study, we have carried out a comparison between the numerical simulation and the analytical solution to a heat conduction and thermal stress problem in a hollow cylinder that has an infinite length, as shown in Fig.1. The inner and outer surfaces of the cylinder are assumed to be at 0^0C initially. The outer surface is subsequently heated to 100^0C, while the inner surface is maintained at 0^0C. The other boundary conditions, material properties and dimensions of the cylinder at the final state are listed below.

$E = 2.07 \times 10^5$ MPa, $\alpha = 1.435 \times 10^{-5}$ mm/mm-°C, $\mu = 0.3$,
$a = 4.76$mm, $b = 15.88$mm, $t_o = 100$°C, $t_i = 0$°C

where E — Young's modulus,
α — thermal expansion coefficient,
μ — Poisson's ratio,
a, b — the inner and outer radius of the cylinder, respectively,
t_o, t_i — the temperature on the inner and outer surface of cylinder, respectively.

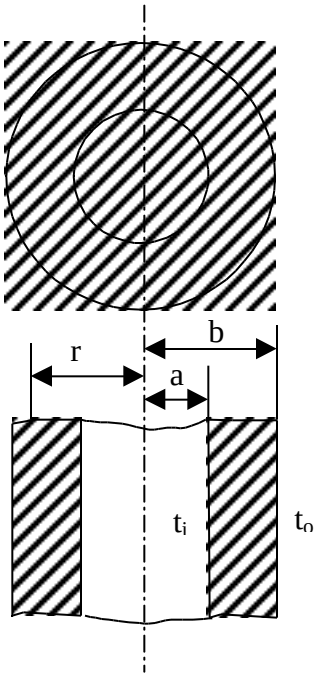

Fig.1 Illustration of model

Analytical solution - The hoop stress σ_t can be expressed as [1]

$$\sigma_t = \frac{E}{1-\mu}\left[\frac{1}{r^2}\int_a^r \alpha t r dr + \frac{r^2+a^2}{r^2(b^2-a^2)}\int_a^b \alpha t r dr - \alpha t\right] \qquad (1)$$

where the equilibrium temperature distribution is represented by the function

$$t = \frac{t_0}{\ln\frac{b}{a}}\ln\frac{r}{a} \qquad (2)$$

With the substitution of equation (2), equation(1) becomes

$$\sigma_t = \frac{E\alpha t_0}{2(1-\mu)\ln\frac{b}{a}}\left[-1-\ln\frac{r}{a}+\frac{b^2}{b^2-a^2}\left(1+\frac{a^2}{r^2}\right)\ln\frac{b}{a}\right] \qquad (3)$$

Using equation (2) with r = 1.5a, we obtain $(t)_{r=1.5a}$ = 33.87 ^{0}C, and using equation (3), we obtain $(\sigma_t)_{r=a}$ = 289.8 MPa at the inner surface and $(\sigma_t)_{r=b}$ = −134.5 MPa at the outer surface.

Solution of numerical simulation - The same problem described above was analyzed using the ANSYS code. The temperature field was simulated using 3-dimensional thermal element solid70 and then the nodal temperatures from the thermal analysis were applied as "body force" loads in the subsequent stress analysis that was modeled using 3-dimensional structural element solid45. The simulation results are as follows:

$(t')_{r=1.5a}$ = 33.84 °C, Discrepancy=0.1%

$(\sigma_t')_{r=a}$ = 292.3 MPa, Discrepancy=0.9%

$(\sigma_t')_{r=b}$ = −131.5 MPa, Discrepancy=2.2%

where the Discrepancy is the relative difference between analytical solution and numerical simulation solution. It is clear that the present numerical simulation provides nearly the identical solution as that provided by the analytical approach.

Modeling of Multi-Materials Laser Densification Process

Four bi-material models including a combination of two laser scanning patterns and two scanning rates (to be detailed below) have been investigated in this study. All of the models investigated have the same geometry. As shown in Fig. 2, the model consists of a dental porcelain (shown in gray or green color) and a dental nickel alloy (shown in dark or red color). The part is built layer-by-layer, i.e. the second bi-material layer is built after fabrication of the first bi-material layer, as shown in Fig. 2. The final size of the part is 20×20×4 mm and the size of every element in the mesh is 2×2×2 mm. The two laser scanning patterns investigated are shown in Fig.3. Note that scanning pattern I has its major scanning direction (i.e. the long scanning direction) parallel to the interface of the bi-material, whereas scanning pattern II has its major scanning direction perpendicular to the interface of the bi-material. The two scanning rates investigated are 10 and 100 μm/s.

The numerical simulation is carried out using the ANSYS code. The simulation approach that has been cross checked with analytical solutions as shown above is used in this simulation. Specifically, 3D thermal element Solid70 is used to simulate the temperature field and 3D structural element Solid45 is then used to simulate the stress field with the nodal temperature obtained from the thermal analysis as the load. Both the dental nickel alloy and the dental porcelain are assumed to have plastic deformation capacities, and simulated using the bilinear kinematic hardening behavior. Furthermore, this bilinear kinematic hardening behavior is a function of temperature. However, the change of Possion's ratio from solid to liquid is neglected. All the material properties used in the model are summarized in Tables I and II. Every element in the model is assumed to be initially solid. An element becomes liquid when its temperature

exceeds its specified melting temperature and solidifies when its temperature becomes lower than its melting point. Thus, the numerical simulation studied herein represents laser processing of multiple solid materials. It is a simplified model for laser processing of multiple powder materials that change to a dense solid body as the fabrication proceeds.

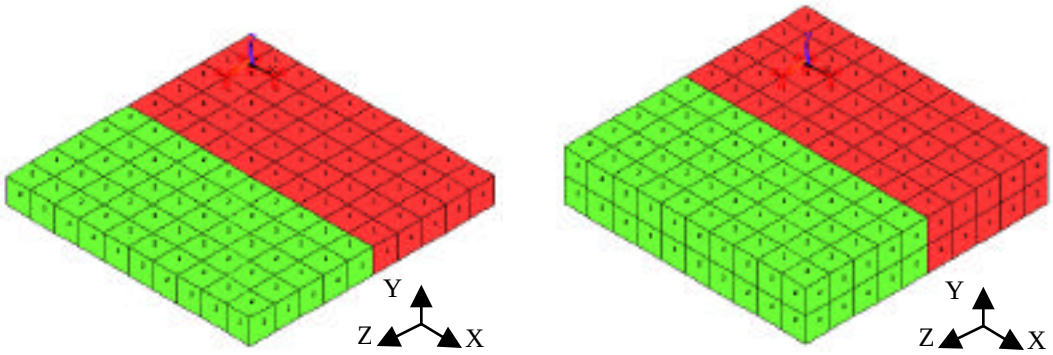

(a) (b)

Fig. 2 Schematic of densification sequence. The first bi-material layer is fabricated in step (a), and the second bi-material layer is built in step (b).

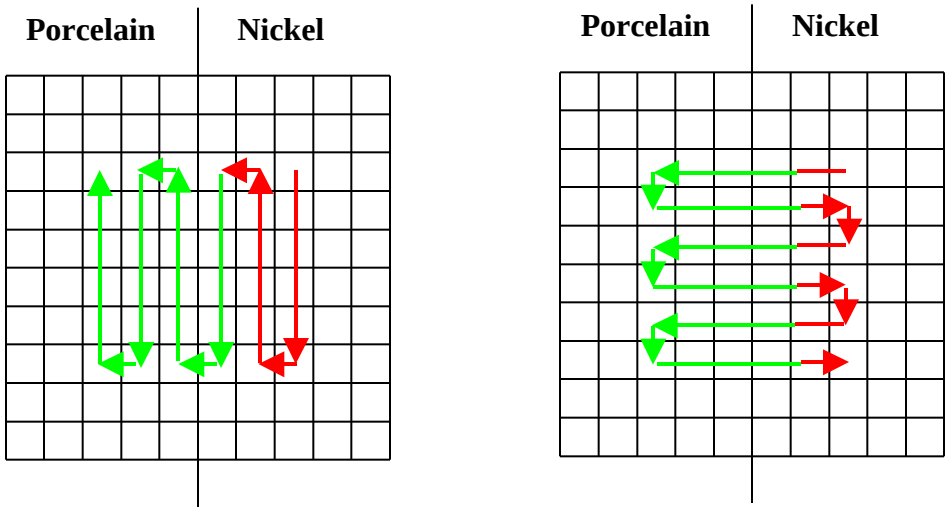

(a) (b)

Fig. 3 The two laser scanning patterns: (a) scanning pattern I and (b) scanning pattern II.

The boundary conditions for modeling are set as follows. The part being built is assumed to be in contact with air and the heat loss through air is approximated through the inclusion of a convection heat transfer coefficient (6×10^{-5} w/mm^{2}K) between the part and the ambient air. The ambient air is assumed to be 300K and the temperature dependence of the convection heat transfer coefficient is neglected. The laser beam heating is modeled as a fixed temperature and moves from a group of surface nodes within the laser beam size 2×2 mm to the next group of surface nodes as defined by the scanning pattern and the scanning rate. The input temperature is set at 1750K when the laser beam scans in the nickel section and 870K in the porcelain section. At the bi-material interface the laser scanning temperature is set at 870K. To avoid rotation and translation of the part during simulation, the node at one of the bottom corners of the part is fixed in X,Y and Z directions. Further, the node next to this fixed node and located at X-axis is fixed in

Y and Z directions, while the node next to the fixed node and located at Y-axis is fixed in X and Z directions. Fixing only one corner allows the part to respond to thermal transient and residual stresses with minimum interference from the boundary condition, and thus stress and distortion analyses can be carried out with reasonable accuracy.

Table I Summary of Material Properties of Nickel Alloy

Temperature (K)	300	470	631	870	1270	1750
Elastic Modulus (MPa)	2.24E5	2.13E5	1.61E5	0.95E5	0.3E5	10
Tangent Modulus (MPa)	1120	1060	805	430	150	0.05
Yield Stress (MPa)	448	402	320	190	60	0.02
Thermal Conductivity (W/mm.K)	0.091	0.071	0.0638	0.069	0.078	0.095
Specific Heat (J/kg.K)	460	485	541	514	552	746
Thermal Expansion Coefficient	13.4E-6	15.1E-6	16.0E-6	17.0E-6	18.7E-6	21.4E-6
Density (g/cm^3)	8.9					
Melting temperature (K)	1728					
Poisson's Ratio	0.33					

Table II Summary of Material Properties of Dental Porcelain

Temperature (K)	300	470	631	870	1270	1750
Elastic Modulus (MPa)	6.93E4	3.16E4	1E4	316	10	10
Tangent Modulus (MPa)	350	160	50	1.6	0.05	0.05
Yield Stress (MPa)	140	63	20	0.6	0.02	0.02
Thermal Conductivity (W/mm.K)	0.0011	0.00136	0.0015	0.0019	0.0027	0.004
Specific Heat (J/kg.K)	754	929	1033	1160	1310	1436
Thermal Expansion Coefficient	2.8E-6	3.1E-6	3.8E-6	5.7E-6	5.7E-6	5.7E-6
Density (g/cm^3)	2.5					
Melting temperature (K)	860					
Poisson's Ratio	0.25					

Numerical Simulation Results

Simulation results of scanning pattern I with scanning speed 10 μm/s are presented in Fig. 4. Fig. 4(a) shows the temperature distribution with the laser beam reaching the final scanning point at the porcelain section. It can be seen that the temperature of the part is approaching the ambient temperature at most of the locations including both metal and porcelain sections except the location heated directly by the laser beam. Thus, the temperature gradient is very small at most of the locations right before turning off the laser beam.

The displacement distribution in Y-direction after the part cools down to room temperature is shown in Fig. 4(b). As can be seen, the distortion of the part is very small, i.e. the largest displacement is about 0.3% of the thickness of the part. Fig. 4(c) and Fig. 4(d) show the stress distributions in X- and Z-direction respectively after the part cools down to room temperature. It can be seen from Fig. 4(c) that the stress along X-direction in nickel near the interface is tensile, whereas the counterpart in porcelain is compressive. This is mainly due to different coefficients of thermal expansion (CTE) between the two materials, as articulated below. At 870K, the stress at the interface is very small because of the stress relaxation of the molten porcelain. However, tensile stresses start to develop in nickel at and near the interface once temperature decreases below 870K because of the higher CTE of nickel. Accompanied with this, compressive stresses develop in porcelain at and near the interface and in nickel at the region opposite to the interface.

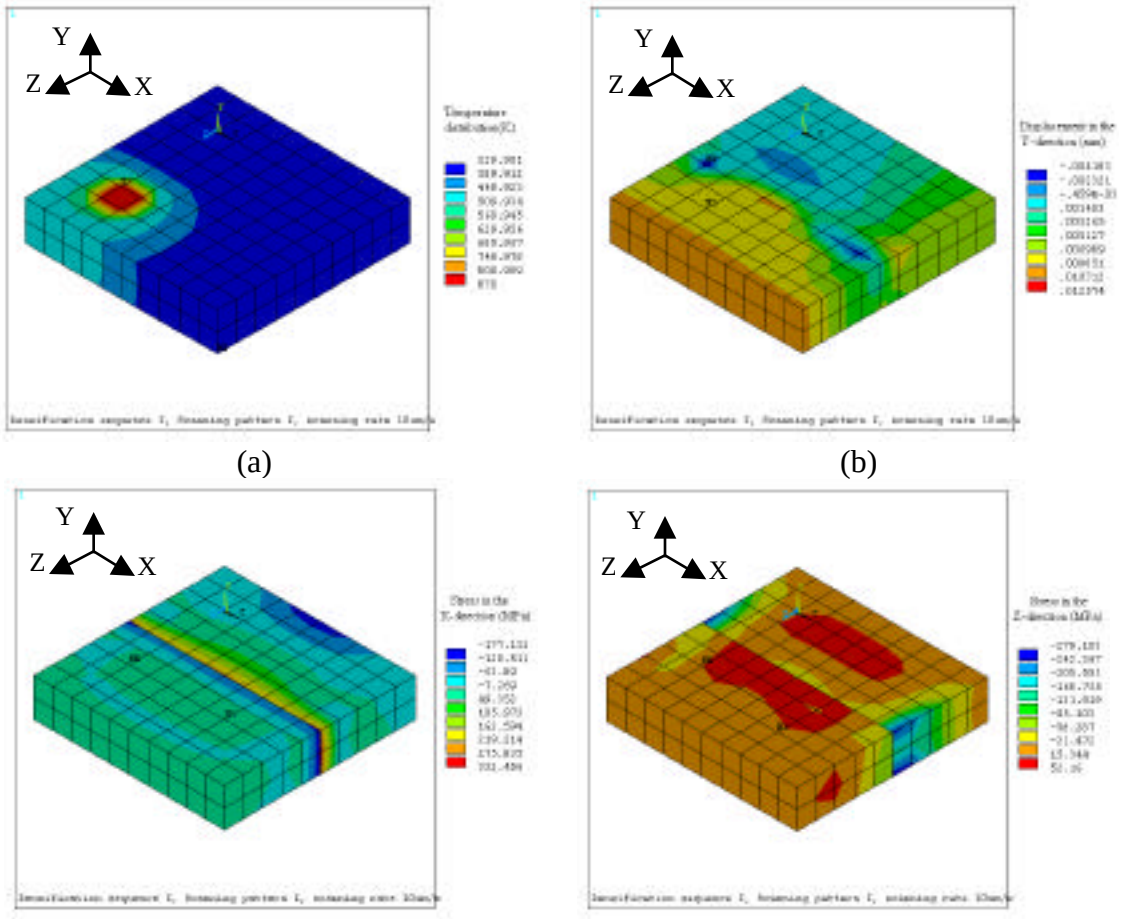

Fig.4 Simulation results of scanning pattern I with scanning speed 10 μm/s. (a) temperature distribution when laser beam scanning the final point and after cooling down to room temperature (b) displacement distribution in Y-direction, (c) stress distribution in X-direction and (d) stress distribution in Z-direction

Fig. 4(d) shows that Z-direction tensile stresses are located in the laser beam scanning path, while compressive stresses are present at both edges of the part perpendicular to the interface. The material under the laser beam is in a molten state during laser scanning. The molten material expands with the solid material around; however, stress build-up is very small because of the presence of the molten material. During cooling down, these molten regions shrink more than the surrounding material. Thus, there are tensile stresses in the laser scanned regions and compressive stresses in the others.

The simulation of scanning pattern I with the fast scanning rate (100 μm/s) indicates that the profiles of temperature, distortion and stress distribution described for the scanning rate of 10 μm/s do not change much. The distortion of the part is also very small and the largest displacement is about 0.5% of the thickness of the part. In comparison with the slow scanning rate (10 μm/s), the tensile and compressive stresses in X-direction change less than 6%. However, the stresses in Z-direction change substantially. There is about 120% increase in tensile stress and 17% decrease in compressive stress.

Simulations of scanning pattern II with both scanning rates (10 μm/s and 100 μm/s) indicate that the stresses and distortion are both larger than those in scanning pattern I. In the

simulations of scanning pattern II, the largest displacement is about 1.5% of the thickness of the part at the slower scanning rate and about 4.5% at the faster scanning rate. Compared with the scanning pattern I at the same scanning rate, the stresses in X-direction increase about 200% in compressive stress and 10% in tensile stress; the stresses in Z-direction increase about 40% in compressive stress and 240% in tensile stress. It is noted that because the laser beam scans across the interface back and forth several times during the process of scanning patter II, the dental porcelain near the interface has the larger distortion and residual stresses.

Finally, the present simulation also indicates that a large portion of the porcelain section has a temperature higher than its melting temperature even when the laser beam is scanning at the neighboring nickel section. Clearly, this is due to the high thermal conductivity of the dental nickel alloy and the high densification temperature (slightly higher than the melting point of the dental nickel alloy) used to densify the nickel section. This result suggests that if the densification sequence investigated in this study is used for dental restoration, the shape and dimension of the porcelain section would be very difficult to control because the porcelain section have become liquid and led to substantial distortion of the shape even before the laser beam reaches the porcelain section. The distortion is especially obvious for scanning pattern II as shown in Fig. 5. Thus, when the melting points of the two materials are substantially different, the densification sequence studied herein should not be adopted. The best way would be to fabricate the high melting material section (e.g. the dental nickel alloy) first, and then the low melting material section (e.g. the dental porcelain).

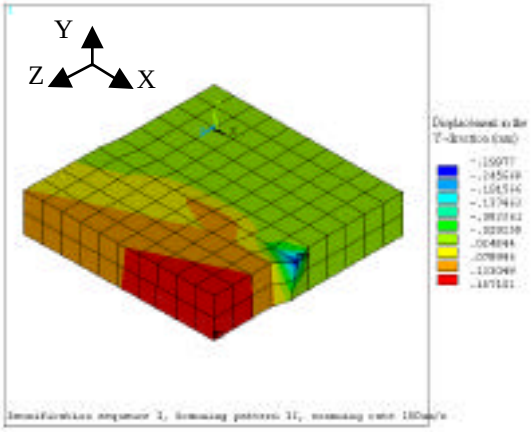

Fig.5 Displacement distribution in Y-direction for scanning pattern II with scanning speed 100μm/s after cooling down to room temperature.

Conclusions

From the models analyzed above we can conclude that

1) A slower scanning rate leads to smaller distortion and stresses in the bi-material part.
2) Scanning pattern I with the major scanning direction parallel to the interface of the bi-material interface can result in a bi-material part with a better quality than scanning pattern II.
3) The densification sequence modeled in this paper is not suited for fabrication of parts made of two materials with the substantially different melting points.

Acknowledgement – The authors gratefully acknowledge financial support provided by the National Science Foundation under Grant No: DMI-9908249.

References

[1] S.Timoshenko, Strength of Materials, Part II--Advancede Theory and Problems, 3rd Edition, D.Van Nostrand Company, Inc., Princeton, New Jersey,1975.